Radar Signal Demixing via Convex Optimization

Youye Xie, Shuang Li, Gongguo Tang, and Michael B. Wakin
Department of Electrical Engineering, Colorado School of Mines, Golden, CO, USA
Email: {youyexie, shuangli, gtang, mwakin}@mines.edu

***Abstract*—The problem of decomposing a signal into components of different structures arises in many applications of signal processing and machine learning. In this paper, we study such a signal demixing problem for airborne radar systems, where the received signal consists of contributions from targets, jammers, and clutter. We promote the structures of the target and jammer components by designing two atomic norms, while we model the clutter signal as lying in a known subspace. This allows the formulation of a convex optimization that is able to separate these components, enabling the localization of targets and jammers as well as the supression of the clutter. Simulations show the superior performance of our approach compared to the classical space-time adaptive processing (STAP) technique.**

I. Introduction

A. Airborne radar systems

Airborne radar systems are widely used in hazardous weather detection, navigation aids, ground mapping and sea searching [1], [2]. Its motion flexibility and capability of wide range imaging provide enormous benefits in these applications. This work focuses on systems with a pulse Doppler radar mounted on an airborne platform. The pulse Doppler radar utilizes the Doppler effect to determine the targets' velocities and the pulse delay ranging to measure the targets' distances [3]. The radar antenna is usually a linear array with uniform spacing. During detection, the transmitter antenna sends out pulses at a constant pulse repetition frequency (PRF) and the returned data is collected over a coherent processing interval (CPI). Within each pulse repetition interval (PRI), the receiver samples the received data and a digital processor performs signal processing to analyze the signal.

A target contributes to the received signal a componenet that depends on the target's azimuth, elevation and velocity relative to the airborne platform and can be located by its spatial and Doppler frequency. Besides the possible target signal, several interferences, particularly those from clutter, jammers, and noise, can be captured by the antenna [4]. The clutter signals are mainly caused by the earth surface and may vary due to the specific surveillance environment. Since the ground clutter covers all searching azimuths and elevations, its pattern may spread over all the spatial and Doppler frequencies [2]. For a stationary radar platform, the clutter pattern is an edge occupying all spatial frequencies but zero Doppler frequency, while for a moving radar platform, the aircraft motion induces a linear relationship between the Doppler frequency and the spatial frequency when the array aligns with platform velocity. The barrage jamming is a tactical artificial signal which distributes over all Doppler frequencies with a fixed spatial frequency at a long range [2].

Space time adaptive processing (STAP), first proposed by Brennan et al. [5], [6], is a well-known adaptive filtering technique to demix the above signals. Based on the estimated interference covariance matrices, STAP attempts to provide high gain on the target spatial and Doppler frequencies while nulling the interferences. Fully adaptive STAP weights all elements and pulses adaptively but suffers from high computational complexity. Alternatively, partially adaptive STAP [7] is proposed to weight adaptively in a smaller manageable space. However, besides the computational complexity, there are other limitations of STAP. First, it is very challenging for STAP to detect targets whose spatial and Doppler frequencies overlap with those for jammers and the clutter. Second, estimating the interference covariance matrices requires multiple-snapshot training data, and the estimation error caused by the sample support issue may lead to extremely small signal-to-interference-plus-noise ratio (SINR) [2]. By leveraging the knowledge of the signal structures, we propose an atomic norm minimization based approach that is able to demix the target, jamming, and clutter signals accurately and stably with single snapshot observations.

B. Atomic norm minimization

Similar to ℓ_1 norm minimization, which promotes sparse models in signal recovery problems, atomic norm minimization promotes sparsity with respect to a dictionary, whose elements (also known as atoms) are potentially indexed by a continuous variable [8]. The flexibility in choosing dictionaries allows the atomic norm minimization framework to model and solve inverse problems involving different signal structures, usually in a statistically optimal way. For example, in line spectral estimation, atomic norm minimization achieves optimal sampling complexity up to logarithmic factors for linear signal recovery [9], [10], has near minimax denoising rate for noisy signal estimation [11], [12], produces frequency estimators whose errors approach the Cramér-Rao lower bound [13], and is able to correct the maximal number of outliers [14], [15]. Moreover, it is also applied to super-resolution problems [16], [17], [18], tensor inverse problems [19] and modal analysis problems [20]. Since the received composite signal consists of signals with known structures, atomic norm minimization can also be applied naturally to the airborne radar demixing problem with dictionaries consisting of target, clutter and jamming atoms.

The paper is organized as follows. In Section II, we present the signal model, formulate the atomic norm optimization problem, and develop its dual problem. In Section III, we

reformulate the atomic norm minimization problem approximately as a semidefinite program (SDP) that can be solved in polynomial time. Preliminary numerical simulations to compare the performances of our approach and the STAP method are presented in Section IV. Finally, we conclude in Section V.

II. Problem Formulation

The data collected by a pulse Doppler radar with an antenna array in a CPI can be preprocessed and arranged into a radar datacube, whose three axes are indexed respectively by the range sample, the pulse number, and the antenna element. Target bearing and velocity estimation within a range bin requires applying signal processing techniques to a space-time slice of the radar datacube with a fixed range gate. The space-time snapshot from a CPI datacube is a matrix whose (i,j)th entry corresponds to the data received by the ith antenna element in the jth PRI [21]. So the column and row contain spatial and temporal variations respectively. Let N be the number of elements in the antenna array and M be the number of pulses within each CPI. We vectorize the space-time snapshot into a $MN \times 1$ vector and model it as,

$$\boldsymbol{y} = \boldsymbol{x}_{\mathrm{T}} + \boldsymbol{x}_{\mathrm{J}} + \boldsymbol{x}_{\mathrm{C}}, \tag{II.1}$$

where $\boldsymbol{x}_{\mathrm{T}}$, $\boldsymbol{x}_{\mathrm{J}}$, $\boldsymbol{x}_{\mathrm{C}}$ represent respectively contributions from targets, jammers, and clutter.

By setting the first array element as the reference, we can define the (normalized) spatial and temporal steering vectors of the phase array respectively as [2], [21]:

$$\boldsymbol{a}_N(f) \triangleq \frac{1}{\sqrt{N}}\left[1, e^{j2\pi f}, \cdots, e^{j2\pi f(N-1)}\right]^\top$$
$$\boldsymbol{a}_M(f) \triangleq \frac{1}{\sqrt{M}}\left[1, e^{j2\pi f}, \cdots, e^{j2\pi f(M-1)}\right]^\top,$$

where f is the spatial or normalized Doppler frequency of the detected object. Spatial frequency is determined by the object's elevation and azimuth angles and the Doppler frequency is determined by the object's velocity relative to the airborne radar. Throughout the paper, we use the subscripts "$\top$", "$*$" and "H" to denote "transpose", "conjugate" and "conjugate transpose", respectively.

For a moving target with a specific angle of arrival and velocity with respect to the airborne radar, the received target signal is correlated both spatially and temporally [21]. More precisely, the array response for a single target is the Kronecker product of its spatial and Doppler steering vectors up to a magnitude scaling. A jammer is spatially correlated but temporally uncorrelated from the radar point of view [2], contributing to the observation the Kronecker product of its temporal samples and the spatial steering vector. In addition, for a well aligned system, the clutter from all angles lies on a linear ridge in the angle-Dopper plane and can be modelled using a subspace, whose dimension P can be determined using Brennan's rule [22]. We assume this subspace is known since it is determined by the platform motion parameters. Let $\mathbf{B} \in \mathbb{C}^{MN\times P}$ be a matrix whose columns form an orthonormal basis for the clutter subspace, and let $\boldsymbol{z} \in \mathbb{C}^{P\times 1}$ be the coefficient vector for the clutter signal component. In sum, with K targets and L jammers, the target, jamming and clutter signal components are given respectively as

$$\boldsymbol{x}_{\mathrm{T}} = \sum_{k=1}^{K} c_k \boldsymbol{a}_M(f_k^{\mathrm{T_D}}) \otimes \boldsymbol{a}_N(f_k^{\mathrm{T_S}}),$$
$$\boldsymbol{x}_{\mathrm{J}} = \sum_{l=1}^{L} d_l \boldsymbol{h}_l \otimes \boldsymbol{a}_N(f_l^{\mathrm{J_S}}), \text{ and } \boldsymbol{x}_{\mathrm{C}} = \mathbf{B}\boldsymbol{z},$$

where c_k, d_l are complex scalar coefficients. Note that we have used "T", "J", "C", "D" and "S" to denote "Target", "Jamming", "Clutter", "Doppler" and "Spatial", respectively. For example, under this notation, $f_k^{\mathrm{T_D}} \in [0,1)$ represents the normalized Doppler frequency for the kth target. The vector $\boldsymbol{h}_l \in \mathbb{C}^M$, scaled to have unit ℓ_2 norm, represents temporal samples of the lth jammer.

Our goal in this work is to separate the target component $\boldsymbol{x}_{\mathrm{T}}$, the jamming signal $\boldsymbol{x}_{\mathrm{J}}$ and the clutter contribution $\boldsymbol{x}_{\mathrm{C}}$ from the received signal $\boldsymbol{y}$ as shown in (II.1), from which we can further extract the target Doppler frequencies $\{f_k^{\mathrm{T_D}}\}$ and spatial frequencies $\{f_k^{\mathrm{T_S}}\}$, the jamming spatial frequencies $\{f_l^{\mathrm{J_S}}\}$, as well as the clutter coefficient vector $\boldsymbol{z}$.

To exploit the target and jamming signals' structures, we define two atomic sets as follows:

$$\mathcal{A}_{\mathrm{T}} \triangleq \left\{\boldsymbol{a}_M(f^{\mathrm{T_D}}) \otimes \boldsymbol{a}_N(f^{\mathrm{T_S}}) :\ f^{\mathrm{T_D}} \in [0,1),\ f^{\mathrm{T_S}} \in [0,1)\right\},$$
$$\mathcal{A}_{\mathrm{J}} \triangleq \left\{\boldsymbol{h} \otimes \boldsymbol{a}_N(f^{\mathrm{J_S}}) :\ f^{\mathrm{J_S}} \in [0,1),\ \|\boldsymbol{h}\|_2 = 1\right\}.$$

Then, the corresponding atomic norms are defined as [8]

$$\|\boldsymbol{x}_{\mathrm{T}}\|_{\mathcal{A}_{\mathrm{T}}} \triangleq \inf\left\{\sum_k |c_k| : \boldsymbol{x}_{\mathrm{T}} = \sum_k c_k \boldsymbol{a}_M(f_k^{\mathrm{T_D}}) \otimes \boldsymbol{a}_N(f_k^{\mathrm{T_S}})\right\},$$
$$\|\boldsymbol{x}_{\mathrm{J}}\|_{\mathcal{A}_{\mathrm{J}}} \triangleq \inf\left\{\sum_l |d_l| : \boldsymbol{x}_{\mathrm{J}} = \sum_l d_l \boldsymbol{h}_l \otimes \boldsymbol{a}_N(f_l^{\mathrm{J_S}})\right\}.$$

Note that both the target signal $\boldsymbol{x}_{\mathrm{T}}$ and jamming $\boldsymbol{x}_{\mathrm{J}}$ are linear combinations of a few atoms from the atomic sets $\mathcal{A}_{\mathrm{T}}$ and $\mathcal{A}_{\mathrm{J}}$. Therefore, we employ the following atomic norm minimization program to separate different signal components from $\boldsymbol{y}$ (and recover the frequencies):

$$\begin{aligned} \underset{\boldsymbol{x}_{\mathrm{T}},\boldsymbol{x}_{\mathrm{J}},\boldsymbol{z}}{\text{minimize}} \quad & \|\boldsymbol{x}_{\mathrm{T}}\|_{\mathcal{A}_{\mathrm{T}}} + \lambda\|\boldsymbol{x}_{\mathrm{J}}\|_{\mathcal{A}_{\mathrm{J}}} \\ \text{subject to} \quad & \boldsymbol{y} = \boldsymbol{x}_{\mathrm{T}} + \boldsymbol{x}_{\mathrm{J}} + \mathbf{B}\boldsymbol{z}. \end{aligned} \tag{II.2}$$

This formulation can be easily adapted to accommodate noise. Define the real inner product as $\langle \boldsymbol{q}, \boldsymbol{y}\rangle_{\mathbb{R}} \triangleq \mathrm{Re}(\langle \boldsymbol{q}, \boldsymbol{y}\rangle) = \mathrm{Re}(\boldsymbol{y}^H\boldsymbol{q})$. The dual atomic norms are defined as

$$\begin{aligned} \|\boldsymbol{q}\|_{\mathcal{A}_{\mathrm{T}}}^* &\triangleq \sup_{\|\boldsymbol{x}\|_{\mathcal{A}_{\mathrm{T}}}\le 1} \langle \boldsymbol{q}, \boldsymbol{x}\rangle_{\mathbb{R}} \\ &= \sup_{f^{\mathrm{T_D}}, f^{\mathrm{T_S}} \in [0,1)} \left|\langle \boldsymbol{q}, \boldsymbol{a}_M(f^{\mathrm{T_D}}) \otimes \boldsymbol{a}_N(f^{\mathrm{T_S}})\rangle\right|, \\ \|\boldsymbol{q}\|_{\mathcal{A}_{\mathrm{J}}}^* &\triangleq \sup_{\|\boldsymbol{x}\|_{\mathcal{A}_{\mathrm{J}}}\le 1} \langle \boldsymbol{q}, \boldsymbol{x}\rangle_{\mathbb{R}} \\ &= \sup_{f^{\mathrm{J_S}} \in [0,1)} \left\|(I_M \otimes \boldsymbol{a}_N^H(f^{\mathrm{J_S}}))\boldsymbol{q}\right\|_2, \end{aligned}$$

where I_M is the identity matrix of size $M \times M$. Then, the dual problem of (II.2) is given as

$$\begin{aligned} \underset{\boldsymbol{q}}{\text{maximize}} \quad & \langle \boldsymbol{q}, \boldsymbol{y} \rangle_{\mathbb{R}} \\ \text{subject to} \quad & \|\boldsymbol{q}\|^*_{\mathcal{A}_{\mathrm{T}}} \leq 1,\ \|\boldsymbol{q}\|^*_{\mathcal{A}_{\mathrm{J}}} \leq \lambda,\ \mathbf{B}^H \boldsymbol{q} = \mathbf{0}. \end{aligned} \tag{II.3}$$

III. SDP Formulation

In this section, we present an SDP approximation for the atomic norm minimization program in (II.2). Define

$$\mathbf{X}_{\mathrm{J}} = \sum_{l=1}^{L} d_l \boldsymbol{a}_N(f_l^{\mathrm{J_S}}) \boldsymbol{h}_l^{\top}$$

as the reorganization of $\boldsymbol{x}_{\mathrm{J}}$ into a matrix of size $N \times M$ such that $\boldsymbol{x}_{\mathrm{J}} = \mathrm{vec}(\mathbf{X}_{\mathrm{J}})$. Denote the atomic set for multiple-measurement line spectral signals as [23]

$$\tilde{\mathcal{A}}_{\mathrm{J}} \triangleq \left\{ \boldsymbol{a}_N(f^{\mathrm{J_S}}) \boldsymbol{h}^H :\ f^{\mathrm{J_S}} \in [0,1),\ \|\boldsymbol{h}\|_2 = 1 \right\}.$$

It follows that

$$\|\boldsymbol{x}_{\mathrm{J}}\|_{\mathcal{A}_{\mathrm{J}}} = \|\mathbf{X}_{\mathrm{J}}\|_{\tilde{\mathcal{A}}_{\mathrm{J}}},$$

implying that $\|\boldsymbol{x}_{\mathrm{J}}\|_{\mathcal{A}_{\mathrm{J}}}$ has an exact SDP representation [23]

$$\|\boldsymbol{x}_{\mathrm{J}}\|_{\mathcal{A}_{\mathrm{J}}} = \inf_{\substack{\boldsymbol{u} \in \mathbb{C}^N \\ \mathbf{W} \in \mathbb{C}^{M \times M}}} \left\{ \frac{1}{2} \mathrm{tr}(\mathrm{Toep}(\boldsymbol{u})) + \frac{1}{2} \mathrm{tr}(\mathbf{W}) : \begin{bmatrix} \mathrm{Toep}(\boldsymbol{u}) & \mathbf{X}_{\mathrm{J}} \\ \mathbf{X}_{\mathrm{J}}^H & \mathbf{W} \end{bmatrix} \succeq \mathbf{0}, \boldsymbol{x}_{\mathrm{J}} = \mathrm{vec}(\mathbf{X}_{\mathrm{J}}) \right\},$$

where $\mathrm{Toep}(\boldsymbol{u})$ is a Toeplitz matrix with $\boldsymbol{u}$ being the first column. We used $\mathrm{tr}(\cdot)$ to denote the trace of a square matrix.

For $\|\boldsymbol{x}_{\mathrm{T}}\|_{\mathcal{A}_{\mathrm{T}}}$, the authors of [24, Proposition 1] derived the following SDP that produces a lower bound:

$$\underset{\substack{\mathbf{T} \in \mathbb{C}^{(8M+1) \times (8M+1)} \\ t \in \mathbb{R}}}{\text{minimize}} \left\{ \frac{1}{2} \mathrm{tr}(\mathrm{bkToep}(\mathbf{T})) + \frac{1}{2} t : \begin{bmatrix} \mathrm{bkToep}(\mathbf{T}) & \boldsymbol{x}_{\mathrm{T}} \\ \boldsymbol{x}_{\mathrm{T}}^H & t \end{bmatrix} \succeq \mathbf{0} \right\},$$

where $\mathrm{bkToep}(\mathbf{T}) \in \mathbb{C}^{MN \times MN}$ is a block Toeplitz matrix generated by $\mathbf{T}$. The SDP representation is exact if the optimal $\mathrm{bkToep}(\mathbf{T})$ has a Vandermonde decomposition.

As a consequence, we can approximately solve the atomic norm minimization program in (II.2) via the following SDP

$$\begin{aligned} \underset{\substack{\boldsymbol{x}_{\mathrm{T}}, \boldsymbol{x}_{\mathrm{J}}, \boldsymbol{z} \\ \mathbf{T}, t, \boldsymbol{u}, \mathbf{W}}}{\text{minimize}} \quad & \frac{1}{2} \mathrm{tr}(\mathrm{bkToep}(\mathbf{T})) + \frac{1}{2} t + \frac{\lambda}{2} \mathrm{tr}(\mathrm{Toep}(\boldsymbol{u})) + \frac{\lambda}{2} \mathrm{tr}(\mathbf{W}) \\ \text{subject to} \quad & \begin{bmatrix} \mathrm{bkToep}(\mathbf{T}) & \boldsymbol{x}_{\mathrm{T}} \\ \boldsymbol{x}_{\mathrm{T}}^H & t \end{bmatrix} \succeq \mathbf{0},\ \begin{bmatrix} \mathrm{Toep}(\boldsymbol{u}) & \mathbf{X}_{\mathrm{J}} \\ \mathbf{X}_{\mathrm{J}}^H & \mathbf{W} \end{bmatrix} \succeq \mathbf{0}, \\ & \boldsymbol{y} = \boldsymbol{x}_{\mathrm{T}} + \boldsymbol{x}_{\mathrm{J}} + \mathbf{B}\boldsymbol{z}. \end{aligned}$$

IV. Simulations

In this section, we apply the atomic norm minimization approach to target estimation for an airborne radar system described in the previous sections and compare it with the classsical STAP algorithm.

A. Experimental setup

The antenna array contains 8 uniform elements with half-wavelength spacing. There are 8 RPI within each CPI so the received signal $\boldsymbol{y}$ for a fixed range gate can be represented by a 64×1 vector. The received signal contains contributions from targets, jammers, the clutter as well as noise.

The spatial frequency of half-wavelength spacing array ranges from -0.5 to 0.5. Without loss of generality, we shift the $f^{\mathrm{T_S}}$ range to $[0, 1)$ to make it consistent with our model in Section II, and similarly for the normalized Doppler frequency. We set the radar antenna array to be aligned with the airborne velocity and the ratio of the platform speed times PRI over array elements spacing to $\frac{1}{2}$. In this case, the clutter appears as a straight diagonal ridge from bottom left to top right on the angle-Dopper plane [2] as shown in Fig. 1. In order to demonstrate the influence of clutter and jamming on target detection, some of target locations on the angle-Dopper plane overlap with the interferences. To be specific, our targets are located at $(0.2, 0.8)$, $(0.4, 0.1)$, $(0.5, 0.5)$, $(0.2, 0.2)$, $(0.7, 0.4)$, $(0.7, 0.7)$, $(0.9, 0.5)$, $(0.7, 0.1)$, $(0.9, 0.9)$, $(0.4, 0.8)$ where the first coordinates are the spatial frequencies and the second are the normalized Doppler frequencies as shown in Fig. 2. The jamming spatial frequencies $f^{\mathrm{J_S}} = \{0.4, 0.7\}$. So all targets with 0.4 and 0.7 spatial frequencies are interfered by the jammer and all the targets on the diagonal line from bottom left to top right are interfered by the clutter as shown in Fig. 3. In addition, complex white noise with zero mean and standard deviation 0.1 is also added.

Since this is a synthetic experiment and the ground-truth frequency parameters of targets, clutter and jamming are known, we can bypass the interference covariance estimation step and compute it precisely. Therefore, the optimal fully adaptive STAP is applied here [2]. However, it should be noted that our atomic approach does not require knowledge of interference frequencies as discussed in the previous sections. The atomic norm minimization is implemented by solving its SDP approximation using CVX [25], [26], an off-the-shelf toolbox for solving convex optimizations.

B. Results and analysis

Ths STAP result is shown in Fig. 3 while the atomic norm minimization demixing results for jamming and targets are shown in Fig. 4 and Fig. 5, respectively. To better illustrate the demixing performance, ground truth target parameters are highlighted by red stars in all figures.

In Fig. 1, it can be seen that targets are buried in the interference. To better examine the target signal magnitudes, we show the ground truth spectral density in Fig. 2, from which one can identify the locations of targets. As a variant of matched filtering, STAP suppresses both the clutter and jamming while enhancing the gain on the targets' locations. In Fig. 3, it can be seen that STAP recovers some of the targets clearly. However, if the targets are interfered with jamming or clutter, STAP can no longer recover them, which may lead to severely low detection rate as demonstrated in our experiment. Atomic norm minimization results are much more

promising. The jamming spatial frequencies are estimated almost perfectly as shown in Fig. 4. Moreover, the targets interfered by jamming are recovered successfully as shown in Fig. 5, but we can not recover targets buried in the clutter since they have the same structure.

We summarize our major empirical findings from all numerical simulations we performed without presenting many of the details of the experimental results due to space limitation. We investigated four different experimental scenarios: (1) targets have frequencies overlapped with both jamming and clutter, as shown in Fig. 1, (2) targets have frequencies only overlapped with jamming, (3) targets have frequencies only overlapped with the clutter, and (4) all the frequencies in targets are well separated from those in jamming and clutter. In all of the above cases, the jamming and clutter signals overlap with each other on the angle-Dopper plane. As a result, the energy of the jamming signals will transfer to the clutter since this will reduce the atomic norm of the jamming component (note the clutter signal is modeled using a subspace and is not penalized in any way). Therefore, we should expect to identify the jamming frequencies accurately but not their magnitude coefficients. In case (2), similarly, we can recover the overlapped targets and jamming frequencies as shown in Fig. 4 and Fig. 5 but not their magnitude coefficients via atomic norm minimization. In case (3), since the clutter signal can also be written as a linear combination of target atoms, with special relations between the spatial and Doppler frequencies, the targets overlapping with the clutter can not be detected. The amount of energy transferred between target and jamming depends on the regularization parameter λ and in our experiment, the parameter in front of $\|\boldsymbol{x}_{\mathrm{T}}\|_{\mathcal{A}_{\mathrm{T}}}$ is eight while it is two for $\|\boldsymbol{x}_{\mathrm{J}}\|_{\mathcal{A}_{\mathrm{J}}}$. Finally, atomic norm minimization can achieve perfect target recovery in case (4).

Fortunately, by recovering the target and jamming frequencies, we can estimate the targets and suppress the jamming and clutter signals as shown in Fig. 5 which is the most important goal for an airborne radar system. Furthermore, the targets overlapping with jamming signals can also be recovered via atomic norm minimization which leads to a higher detection rate and makes it more robust in strong jamming environments compared to STAP.

V. Conclusion

We proposed an atomic norm minimization approach to solve the airborne radar system demixing problem. We defined two atomic norms that are able to exploit target and jammer signal structures, and modeled the clutter as living in a known subspace. This allowed the formulation of demixing as a convex atomic norm regularization problem. We derived an SDP to approximately solve the atomic norm minimization. Compared to the fully adaptive STAP, our approach can recover the targets that overlapped with jamming, which leads to a higher detection rate without the need to estimate the inference covariance matrix. Numerical simulation shows that our approach outperforms STAP in several aspects. We leave the development of theoretical performance guarantees for the proposed approach to the future work.

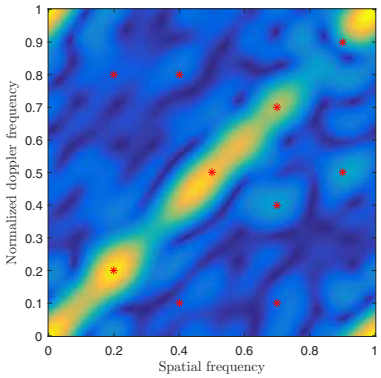

Fig. 1. The spectrum of the composite received signal $\boldsymbol{y}$ which consists of target, clutter, jamming and noise contributions. Both the target and clutter signal coefficients are generated from complex standard normal distributions. The jamming signal coefficients are generated by a real standard uniform distribution random variable on the open interval $(0, 5)$.

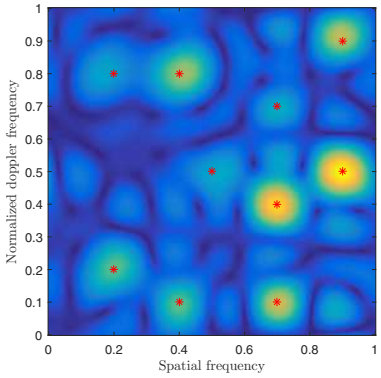

Fig. 2. The spectrum of the targets-only signal (the ground truth) seen by the airborne radar. Targets have varied signal amplitudes since the types of targets may influence the echo signal strength in reality.

Acknowledgment

This work was supported by NSF CAREER grant CCF-1149225, NSF grant CCF-1409258, and NSF grant CCF-1464205.

References

[1] G. W. Stimson, *Introduction to airborne radar*. SciTech Pub., 1998.
[2] J. Ward, "Space-time adaptive processing for airborne radar," 1998.
[3] C. Alabaster, *Pulse Doppler Radar*. The Institution of Engineering and Technology, 2012.
[4] D. K. Barton, "Modern radar system analysis," *Norwood, MA, Artech House, 1988, 607 p.*, vol. 1, 1988.
[5] L. E. Brennan and L. Reed, "Theory of adaptive radar," *IEEE Transactions on Aerospace and Electronic Systems*, no. 2, pp. 237–252, 1973.
[6] L. Brennan, J. Mallett, and I. Reed, "Adaptive arrays in airborne mti radar," *IEEE Transactions on Antennas and Propagation*, vol. 24, no. 5, pp. 607–615, 1976.
[7] H. Wang and L. Cai, "On adaptive spatial-temporal processing for airborne surveillance radar systems," *IEEE Transactions on Aerospace and Electronic Systems*, vol. 30, no. 3, pp. 660–670, 1994.

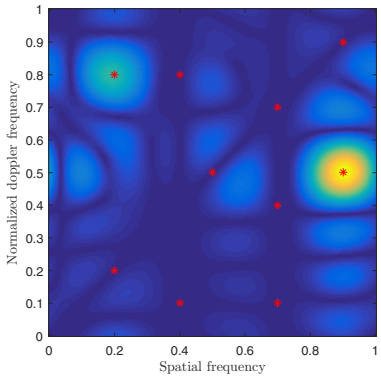

Fig. 3. Space time adaptive processing (STAP) result. Clutter and jamming are suppressed while targets outside the interferences remain.

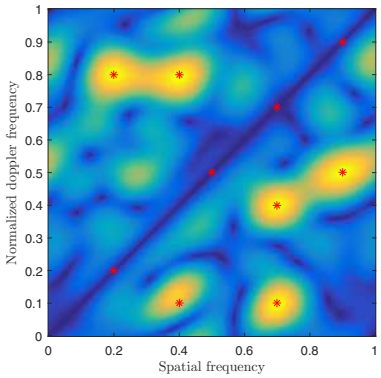

Fig. 5. Atomic norm minimization recovers targets outside the clutter ridge. In particular, the targets interfered by jamming are also recovered.

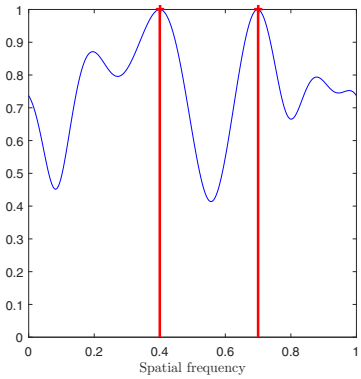

Fig. 4. Atomic norm minimization demixing result for jamming. The ground-truth jamming spatial frequencies are indicated by the red stems while according to the duality theory the estimated jamming frequencies coincide with the places where the blue dual polynomial curve achieves 1.

[8] V. Chandrasekaran, B. Recht, P. A. Parrilo, and A. S. Willsky, "The convex geometry of linear inverse problems," *Foundations of Computational Mathematics*, vol. 12, no. 6, pp. 805–849, 2012.

[9] G. Tang, B. N. Bhaskar, P. Shah, and B. Recht, "Compressed sensing off the grid," *IEEE Transactions on Information Theory*, vol. 59, no. 11, pp. 7465–7490, 2013.

[10] S. Li, D. Yang, G. Tang, and M. B. Wakin, "Atomic norm minimization for modal analysis from random and compressed samples," *arXiv preprint arXiv:1703.00938*, 2017.

[11] G. Tang, B. N. Bhaskar, and B. Recht, "Near minimax line spectral estimation," *IEEE Transactions on Information Theory*, vol. 61, no. 1, pp. 499–512, 2015.

[12] B. N. Bhaskar, G. Tang, and B. Recht, "Atomic norm denoising with applications to line spectral estimation," *IEEE Transactions on Signal Processing*, vol. 61, no. 23, pp. 5987–5999, 2013.

[13] Q. Li and G. Tang, "Approximate support recovery of atomic line spectral estimation: A tale of resolution and precision," *arXiv preprint arXiv:1612.01459*, 2016.

[14] C. Fernandez-Granda, G. Tang, X. Wang, and L. Zheng, "Demixing sines and spikes: Robust spectral super-resolution in the presence of outliers," *arXiv preprint arXiv:1609.02247*, 2016.

[15] G. Tang, P. Shah, B. N. Bhaskar, and B. Recht, "Robust line spectral estimation," in *2014 48th Asilomar Conference on Signals, Systems and Computers*, pp. 301–305, IEEE, 2014.

[16] E. J. Candès and C. Fernandez-Granda, "Towards a mathematical theory of super-resolution," *Communications on Pure and Applied Mathematics*, vol. 67, no. 6, pp. 906–956, 2014.

[17] G. Tang, "Resolution limits for atomic decompositions via markov-bernstein type inequalities," in *Sampling Theory and Applications (SampTA), 2015 International Conference on*, pp. 548–552, IEEE, 2015.

[18] D. Yang, G. Tang, and M. B. Wakin, "Super-resolution of complex exponentials from modulations with unknown waveforms," *IEEE Transactions on Information Theory*, vol. 62, no. 10, pp. 5809–5830, 2016.

[19] Q. Li, A. Prater, L. Shen, and G. Tang, "Overcomplete tensor decomposition via convex optimization," in *Computational Advances in Multi-Sensor Adaptive Processing (CAMSAP), 2015 IEEE 6th International Workshop on*, pp. 53–56, IEEE, 2015.

[20] S. Li, D. Yang, G. Tang, and M. B. Wakin, "Atomic norm minimization for modal analysis from random and compressed samples," *arXiv preprint arXiv:1703.00938*, 2017.

[21] M. A. Richards, *Fundamentals of radar signal processing*. Tata McGraw-Hill Education, 2005.

[22] L. Brennan and F. Staudaher, "Subclutter visibility demonstration," tech. rep., Tech. Rep., RL-TR-92-21, Adaptive Sensors Incorporated, 1992.

[23] Y. Li and Y. Chi, "Off-the-grid line spectrum denoising and estimation with multiple measurement vectors," *IEEE Transactions on Signal Processing*, vol. 64, no. 5, pp. 1257–1269, 2016.

[24] Y. Chi and Y. Chen, "Compressive recovery of 2-d off-grid frequencies," in *2013 Asilomar Conference on Signals, Systems and Computers*, pp. 687–691, IEEE, 2013.

[25] M. Grant and S. Boyd, "CVX: Matlab software for disciplined convex programming, version 2.1." http://cvxr.com/cvx, Mar. 2014.

[26] M. Grant and S. Boyd, "Graph implementations for nonsmooth convex programs," in *Recent Advances in Learning and Control* (V. Blondel, S. Boyd, and H. Kimura, eds.), Lecture Notes in Control and Information Sciences, pp. 95–110, Springer-Verlag Limited, 2008. http://stanford.edu/~boyd/graph_dcp.html.